COBEM 2021 26th International Congress of Mechanical Engineering
November 22-26, 2021, Virtual Congress, Brazil

COB-2021-0893 BUBBLE PATTERN RECOGNITION FROM PARTICLE IMAGE VELOCIMETRY (PIV) IMAGES USING A DEEP-LEARNING-BASED IMAGE PROCESSING TECHNIQUE

Rafael F. L. de Cerqueira[1]
Marco A. Cerutti
Emilio E. Paladino
SINMEC - Computational Fluid Dynamics Lab Mechanical Engineering Department, Federal University of Santa Catarina, 88040-900 - Florianopolis - SC - Brazil
rafaelfc@unicamp.br
mcerutti@sinmec.ufsc.br
paladino@sinmec.ufsc.br

[1] Currently at the Center for Petroleum Studies, University of Campinas, Cora Coralina Street, 350, Campinas, São Paulo, Brazil

Abstract. *This work presents a deep-learning image processing tool for the analysis of bubbly flows using Particle Image Velocimetry (PIV) technique. The measurement in gas-liquid bubbly flows is a challenging task, mostly due to the laser light's dispersion caused by the gas-liquid interfaces. A common solution is the use of fluorescent seeding particles associated with a bandpass filter for the laser light, which consists of the PIV technique combined with laser-induced fluorescence (LIF), known as PIV/LIF. When using the additional LIF setup, the interfaces are not fully removed from the acquired images, once they still reflect the fluoresced light. This is not beneficial for the PIV acquisitions, since the measurement technique is based on the movement of tracer particles located in the liquid phase. In the past few years, several authors proposed image processing techniques to alleviate this problem and enable the use of the PIV technique for the characterization of gas-liquid bubbly flows. The present work aims to use this drawback, the appearance of the gas-liquid interface in the PIV acquisitions, as a tool to completely characterize the gas phase. Due to the high noise level from the seeding particles into the dispersed bubble interface, which appears as bright particles in the acquired PIV images, traditional computer vision techniques algorithm fails to detect the dispersed bubbles in the images. Hence, the current work presents a novel deep-learning-based imaging processing technique based on the use of a U-Net Convolutional Neural Network (CNN), employed for semantic image segmentation tasks, and a Faster-RCNN, a region-based object detection convolutional neural network. Additionally, a second CNN is used to reconstruct the dispersed gas bubble interface through ellipsoids. Thanks to the bubble reconstruction capability of the proposed technique, a Labelled Object Velocimetry (LOV) algorithm can be incorporated into the developed framework to calculate the instantaneous velocities of the dispersed bubbles from the two recorded PIV frames. In this way a full characterization of the liquid and gas flow field can be performed only from the PIV acquisitions. The developed methods are tested with PIV acquisitions from a set of upward laminar and turbulent vertical bubbly gas-liquid flows. Ensemble average bubble velocity profiles are calculated in different experimental conditions, showing that the global void fraction affects the gas velocity profiles.*
Keywords: *bubbly flow, PIV, LOV, deep-learning*

1. INTRODUCTION

The use of the Particle Image Velocimetry (PIV) technique, due to its multi-dimensional resolution and non-intrusive characteristics, allows engineers and researchers to study flows in rich detail. In gas-liquid bubbly flows, information about the liquid phase velocity field is of fundamental importance to characterize the flow structure. However, the liquid velocity field measurement in gas-liquid flows is not straightforward, mainly due to the laser light scattering by the interfaces in different and unwanted directions. This light scattering effect obfuscates the light reflected from seeding particles and eventually may damage the camera sensor.

The PIV/LIF technique uses fluorescent particles that absorb the laser light (typically at 532 nm) and emit light in a higher length and a band-pass optical filter that filters the laser light to the camera, capturing the fluoresced light. However, fluoresced light still gets reflected at the interfaces and is scattered out of the laser plane, illuminating dispersed bubbles positioned out of the focal and laser plane. Due to these optical effects, while acquiring the PIV images, the gas bubbles appear on the raw PIV images with different structure, such as halos, auras or diffused circles. These structures introduce spurious contributions into the PIV processed results for the liquid velocity fields.

Therefore, in the last few years, different authors Bröder and Sommerfeld (2007); Zhou *et al.* (2013); Cerqueira *et al.* (2018); Bueno *et al.* (2018) proposed optical and image processing techniques to mitigate those effects and remove the

gas-phase contribution on the liquid velocity fields. In recent years, some authors proposed the use of deep-learning techniques for image processing technique for bubbly flows with the shadowgraphy method Haas *et al.* (2020); Torisaki and Miwa (2020); Serra *et al.* (2020) and also through the planar laser-induced fluorescence (PFBI) Poletaev *et al.* (2020) method. In general, those deep-learning techniques present similar or better results compared to the "classical" image processing methods based on analytical (e.g. Cerqueira *et al.* (2018)). Recently, Chun-Yu *et al.* (2021) used a deep-learning technique to enable the study of an object entering a liquid surface through the PIV technique. The deep-learning technique described in Chun-Yu *et al.* (2021), generated a dynamic mask from the raw PIV images, which was superimposed into the raw image, allowing the discrimination of the different phases.

The measurement of the gas phase is also important for the complete characterization of the flow structure, and it is usually done through the analysis of high-speed camera images with the help of the shadowgraphy technique. Through this illumination setup, a backlight is positioned on the back of the test section perpendicular to the camera lens. This allows the acquisition of high-contrast images, where the gas-liquid interface is clearly visible. After identifying and labelling the bubbles in two consecutive images, a Particle Tracking Velocity algorithm can be used to determine the bubble velocities and its size distribution (Cerqueira *et al.*, 2018; Cerqueira and Paladino, 2021). Another option is to employ the recent method proposed by Laupsien *et al.* (2021), which is based on spatial correlations similar to those used in Particle-Image Velocimetry (PIV) called Labelled Object Velocimetry (LOV). According to the authors this method has some advantages over the traditional PTV, being the main ones, the fact that there is no need of labelling the objects in the two images, as the correlation identifies the object position in the second frame. In addition, it can be applied to deformable objects, as the tracking is not based on the geometric centre of the object as in the PTV technique.

Due to the advantages associated with the use of deep-learning techniques in image processing, a method for the identification of bubbles in PIV images of bubbly flows, based on image segmentation using a U-Net convolutional neural network Ronneberger *et al.* (2015) was recently proposed in Cerqueira *et al.* (2021). This method is used to create a binary mask that discriminates the flow phases in raw PIV images of bubbly flows before applying the PIV algorithm to the images, removing the spurious contribution of the gas phase from the processed liquid velocity fields. In this paper, we extend this technique using the mask obtained from U-Net segmentation as input in a F-RCNN, which is able to detect the dispersed bubble positions and attribute a label to each bubble. Then, the bounding box returned by the F-RCNN and the binary mask image from the UNET are used as an input to the LOV technique, which returns the velocity of each individual dispersed bubble. In addition, the detected dispersed bubbles shape is approximated by ellipses through a CNN-based shape regressor, being able to determine the bubble diameter distribution.

The proposed deep-learning-based image processing technique is applied to PIV/LIF acquisitions from experiments carried in different superficial gas and liquid velocities in a vertical bubbly flow experimental setup (Cerqueira *et al.*, 2018). The average gas velocity obtained from the technique described in the present work is compared against the results of Cerqueira *et al.* (2018), acquired through a shadowgraphy-based PTV algorithm. Owning to the advantage of the planar characteristics of the presented method, average gas velocity profiles are obtained in different experimental conditions to illustrate the effect of the superficial gas velocity on those profiles.

2. EXPERIMENTAL SETUP

The experimental setup allows for the generation of a single-phase liquid stream or bubbly flow in a straight vertical duct, where the water and air flow rates, and thus, the superficial velocities, can be independently controlled.The test section consists of a transparent pipe with $D = 26.2$ mm internal diameter and $L = 2.0$ m length. This experimental setup was used in previous investigations from the group, and the measurement apparatus was validated on several occasions Cerqueira *et al.* (2018, 2019); Cerqueira and Paladino (2021).

The experimental apparatus is schematically depicted in Fig. 1.

At the PIV measurement section, a box constructed with transparent acrylic, made with 8 plane faces filled with water, is included to minimize optical distortion. A two-phase bubbly flow is generated at the bottom of the test section by combining a liquid stream (tap water), driven by a centrifugal pump, and air from the compressed air line from the building. The air is treated to eliminate oil, and solid particles and pressure is maintained constant at the injection point through a pressure regulating valve, making it independent of the line demand. The gas is injected at the bottom of the tube through a porous gas diffuser in order to control the sizes of the dispersed bubbles. The gas flow rate is measured by two OMEGA FL-3802ST/FL-3861SA flow meters with ranges of 81.4-814.0 standard mL/min and 26.3-263.0 standard mL/min, both with $\pm 2.0\,\%$ full-scale accuracy. The air flow rate is controlled by a needle valve located after the rotameters. In order to correct the gas superficial velocity due to gas expansion, pressure and temperature sensors were installed downstream of the needle valve. As the return to the reservoir consists of a relatively short (~ 0.5 m), and 50.0 mm internal diameter duct, and the reservoir is opened to the atmosphere, it was assumed that the pressure at the test section was close to the atmospheric pressure.

The water flow rate is measured by an OMEGA FL46303 flow meter with a range of 1.00-7.50 l/min with $\pm 5.0\,\%$ full-scale accuracy. The liquid flow rate is controlled by a frequency inverter connected to the electric water pump motor.

Details regarding the experimental setup can be found in Cerqueira *et al.* (2018, 2019); Cerqueira and Paladino (2021).

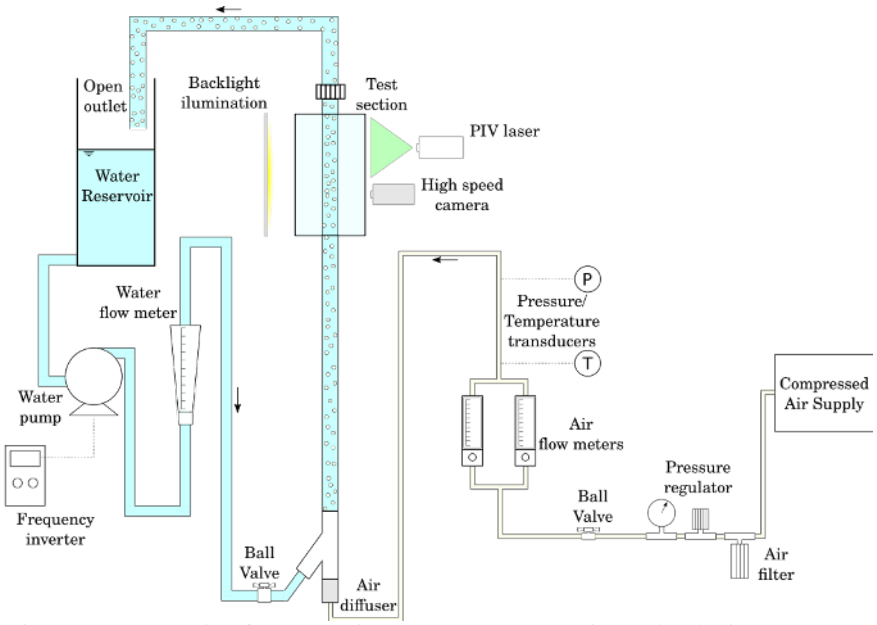

Figure 1: Schematic of the experimental setup. Cerqueira and Paladino (2021)

3. DEEP-LEARNING MODELS

In the present work, the deep-learning methods and image processing algorithms were developed in the Python programming language. The image processing routines were implemented using the OpenCV library Bradski (2000). For the deep-learning model development, the Keras Chollet *et al.* (2015) framework with a Tensorflow Abadi *et al.* (2015) backend was employed.

3.1 U-Net

The U-Net is a convolutional network architecture for fast and precise segmentation of images Ronneberger *et al.* (2015). As opposed to typical encoder-decoder neural network architectures Bank *et al.* (2020), the encoder and decoder layers are directly connected. This architecture helps the network to recover information lost during the max-pooling operations from the encoder module. For more details regarding the U-Net convolutional network architecture, the reader may refer to the original implementation Ronneberger *et al.* (2015).

In order to train the U-Net convolutional network, raw PIV images were manually labeled to create the training datasets. This labelling process was done through the ImageJ software Rasband *et al.* (1997), where all the bubbles present in the images were identified and their shapes approximated by manually fitted ellipses.

For the U-Net model training, the raw PIV image and the binary masks were used as input to the model, as schematically depicted in Fig. 2. The procedure is similar to the one described in Cerqueira *et al.* (2021), however in the present work, instead of approximating the dispersed bubble as “full” ellipsoids, which are used to mask the PIV images for the determination of liquid phase velocity, they are approximated as outline ellipsoid contours. Further, those contours are used for the determination of bubbles velocities and sizes.

Details regarding the U-Net model and the architecture used in the present work are shown in Cerqueira *et al.* (2021), where the current authors developed and tested the U-Net model as a dynamic mask to remove the dispersed bubbles in bubbly flow PIV images.

3.2 F-RCNN

The architecture of Faster R-CNN is a single-stage model that is fast and accurate at detecting and classifying objects contained in images. It consists of 2 modules, a region proposal network (RPN) which provides regions where objects are located, and a mixed classifier and regressor CNN which returns the detected object class scores in addition to its bounding-box. The RPN model resembles a classical CNN, but in the last convolutional feature maps a number of positions in the image are chosen to house "anchors". These anchors are a set of rectangular boxes of varying sizes and aspect that are evaluated as containing or not an object. These regions are classified and a bounding box is fitted to the object.

The F-RCNN model was trained from the labeled datasets and the U-Net described in the previous paragraphs. First, a binary mask was created from the U-Net and then, the bounding box of each labelled dataset was used to train the

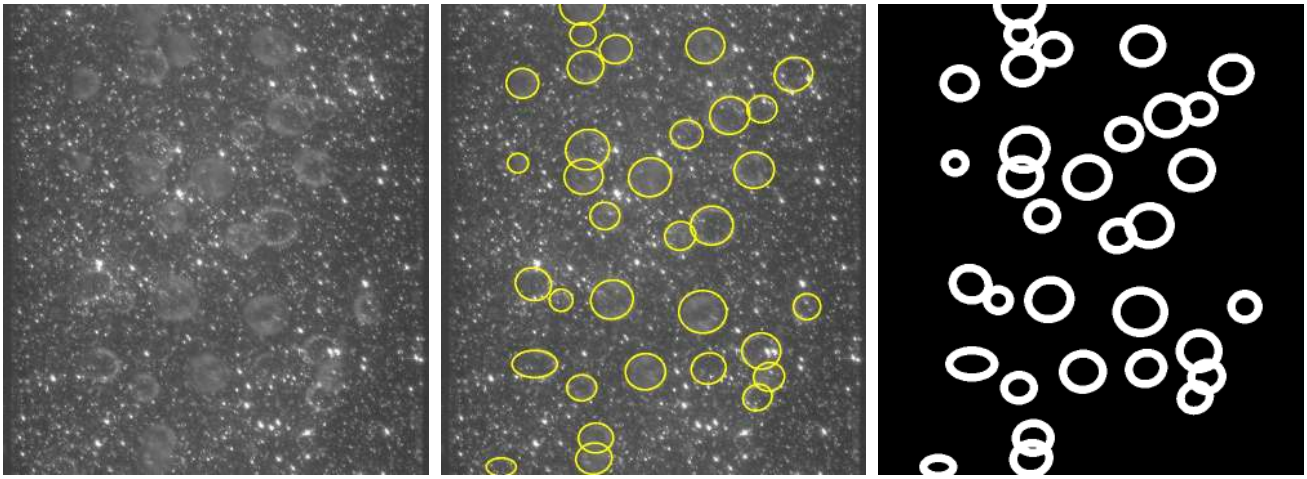

(a) (b) (c)

Figure 2: Different steps during the U-Net dataset creation: a) raw bubbly flow image acquired during experiments by the PIV setup; b) PIV raw image with the identified bubbles labelled as ellipse through the ImageJ software; c) binary mask from the manually identified bubbles from image b). During training, images a) and c) are used as input to the U-Net model.

F-RCNN model. Therefore, the F-RCNN could detect the exact position of the dispersed bubbles in the image. Initial tests were conducted to train the F-RCNN model by using the raw PIV images. However, by using this approach, the model could not detect the dispersed bubbles in the images. Hence, identification through a U-Net processed image was preferred. Figure 3 illustrates the different steps used to train the F-RCNN model.

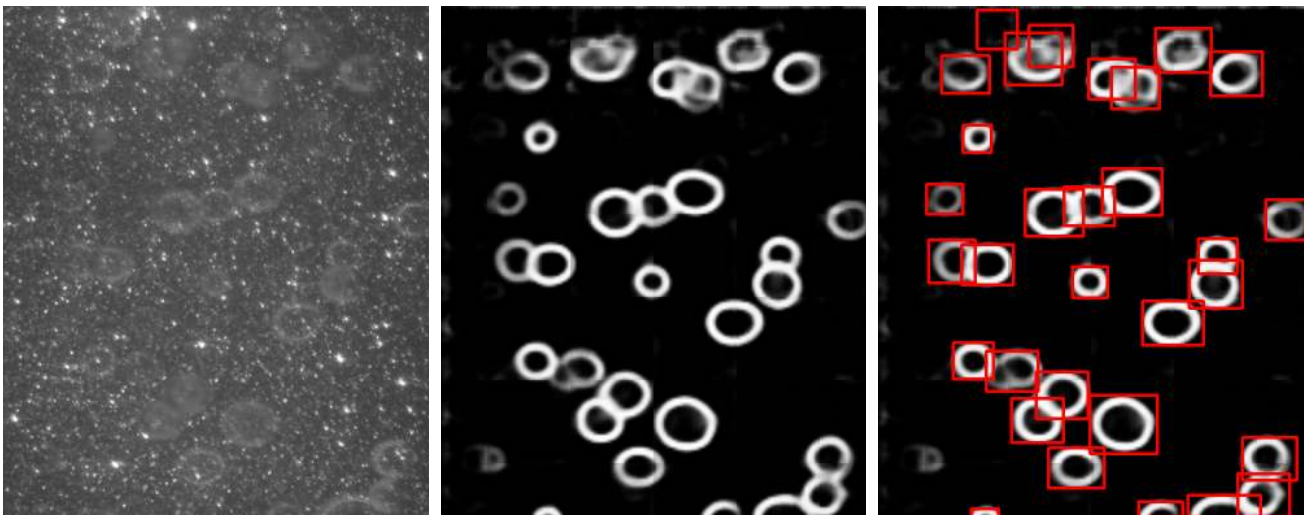

(a) (b) (c)

Figure 3: Different steps for training the F-RCNN: a) raw bubbly flow image acquired during experiments by the PIV setup; b) U-Net generated binary mask with the dispersed bubbles represented by elliposoid contour outlines; c) bounding boxes from the labelled dataset. Images a) and the bounding box of all the labelled dispersed bubbles (shown in image c)) are used during the F-RCNN model training.

3.3 CNN Shape Regressor

After locating the bubbles using the F-RCNN model, a CNN model was trained to regress and fit ellipses in the located bubbles. The training data was sourced from the manually fitted ellipses used to create the masks for training the U-Net model. When trained, the bubble shape regressor is able to output the coordinates of the bubbles' centroids, the length of the bubbles' major and minor axes' as well as the angle of the axes relative to the image coordinates system. As in the F-RCNN model, the shape regressor CNN produced better results when using the U-Net generated binary masks over using the raw PIV images. Therefore, the use of U-Net is of fundamental importance when dealing with "noisy" such as

those used by the PIV technique. Figure 4 illustrates the returned ellipse in different situations.

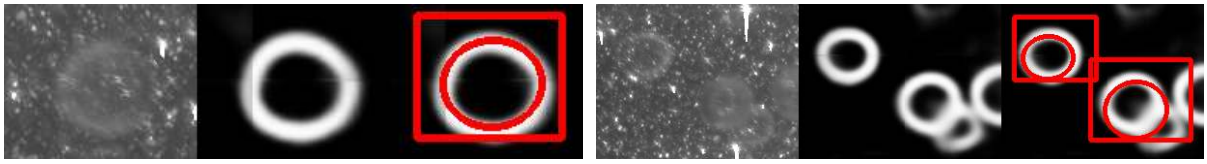

(a) (b)

Figure 4: Examples of the returned ellipses from the CNN used for the dispersed bubble shape regression.

3.4 Deep-Learning Model Overview

In order to preset a better comprehension of the mentioned techniques and the approach adopted in the present work, Fig. 5 presents a schematic of the Deep-Learning model used here.

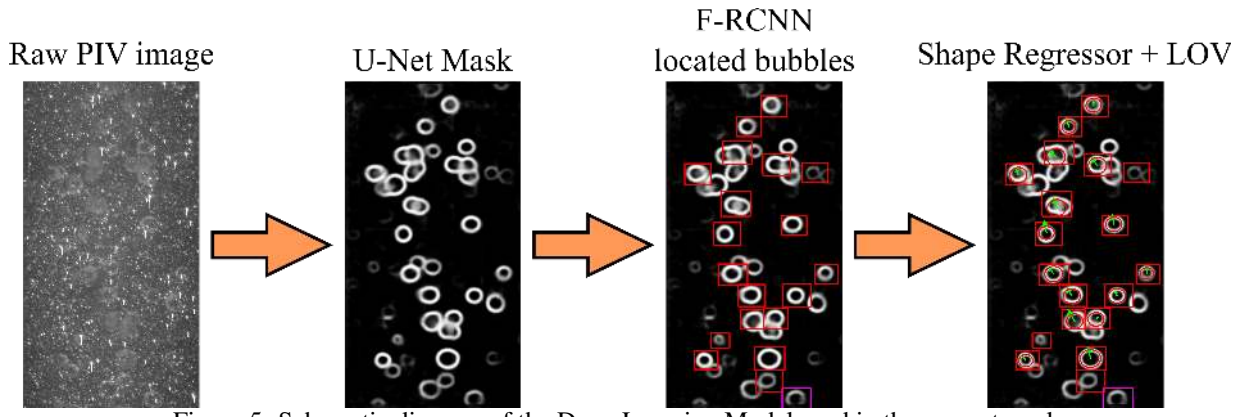

Figure 5: Schematic diagram of the Deep-Learning Model used in the present work.

As observed in Fig. 5, the raw PIV image creates an U-Net binary mask, which is then used to locate the bubbles and reconstruct their shape. Here, it is important to state that for each PIV acquisition, two U-Net masks are created, one for each PIV frame, where the time interval is known and set during the PIV experiments. Thus, the two U-Net masks are used to compute the gas bubble velocity, as described in the next section.

4. Labelled Object Velocimetry

After classifying the entire set of contours in a given image, the Labelled Object Velocimetry (LOV) technique (Laupsien *et al.*, 2021) was used to calculate the drop displacement. The LOV is based on the spatial correlation of two frames and it is similar to the Particle-Image Velocimetry (PIV), but instead of using images where tracer particles are present, the technique uses grey level images. In Laupsien *et al.* (2021), the authors use the technique to compute the instantaneous velocity of gas bubbles from shadowgraphy images. First, the authors binarize the image and detect the bubble contours. Then, bounding boxes are fitted around the found contours. These bounding boxes have their height and width extended by a few pixels, forming a "search area". The coordinates and dimensions of these extended regions are used to extract portions of the next frame. Finally, the image extracted by the original bounding box is correlated against this extended area in the next frame. This correlation procedure then returns the velocity of each contour, which in the original implementation of Laupsien *et al.* (2021) represents a gas bubble.

In the present work, the LOV method is modified to use the bounding box returned by the F-RCNN model and the images from the U-Net model are used to compute the cross-correlation.

5. RESULTS

5.1 Experimental Matrix

In the present work, some of the experimental points from the PIV recordings from Cerqueira *et al.* (2018) were used to develop and assess the deep-learning models described in this work. These experimental conditions are shown in Tab. 1, where the liquid j_l and gas j_g superficial velocities were calculated based on the gas and liquid flow rate measurements. The parameter β corresponds to the gas to total superficial velocities relationship, $\beta = j_g/(j_g + j_l)$. Details regarding the gas volume fraction $\overline{\langle \alpha_g \rangle}$ and the mean equivalent spherical bubble diameter $\overline{\langle d_b \rangle}$ calculation are given in Cerqueira *et al.*

(2018).

Table 1: Test Matrix of the experiments from Cerqueira *et al.* (2018) processed by the model described in the present work.

Experiment No.	$j_l\ [m/s]$	$j_g\ [m/s]$	$\beta\ [-]$	$\overline{\langle \alpha_g \rangle}\ [-]$	$\overline{\langle d_b \rangle}\ [mm]$
1	$3.09 \cdot 10^{-2}$	$2.38 \cdot 10^{-3}$	0.084	0.013	1.78
2		$5.89 \cdot 10^{-3}$	0.160	0.029	1.81
3	$21.64 \cdot 10^{-2}$	$2.38 \cdot 10^{-3}$	0.013	0.007	1.79
4		$9.66 \cdot 10^{-3}$	0.043	0.025	1.64

5.2 Visual Analysis

In order to assess the results of the proposed deep-learning model introduced in the present work, Fig. 6 present the result of its application in two different experimental conditions of Tab. 1. As observed, the U-Net model is able to create a binary image of the raw PIV acquisitions where the outline of the dispersed bubbles are clearly visible, even in cases where the bubbles are overlapping. In addition, the F-RCNN is capable of identifying most of the bubbles present in the binary image. When the dispersed bubbles are identified, the shape regressor CNN can approximate its shape by an ellipsoid. In Fig. 6, not all the identified bubbles have an instantaneous velocity vector. This is due to the LOV technique, which is based on a spatial correlation technique. In the present work, if the correlation peak has a low signal-to-noise ratio (SNR), the instantaneous velocity is discarded.

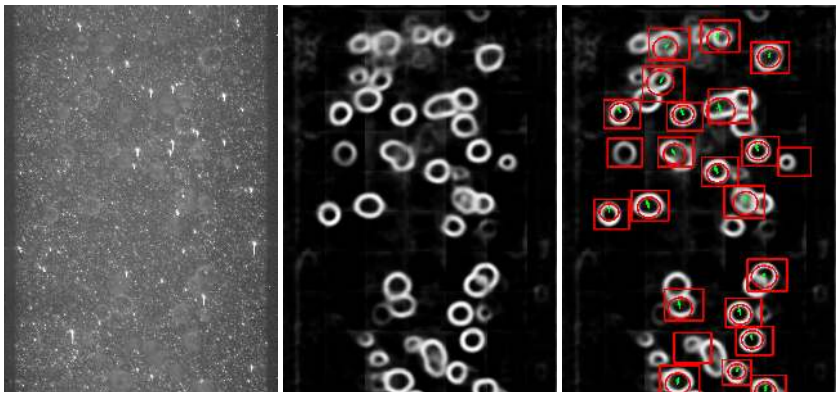

(a) Exp. 1

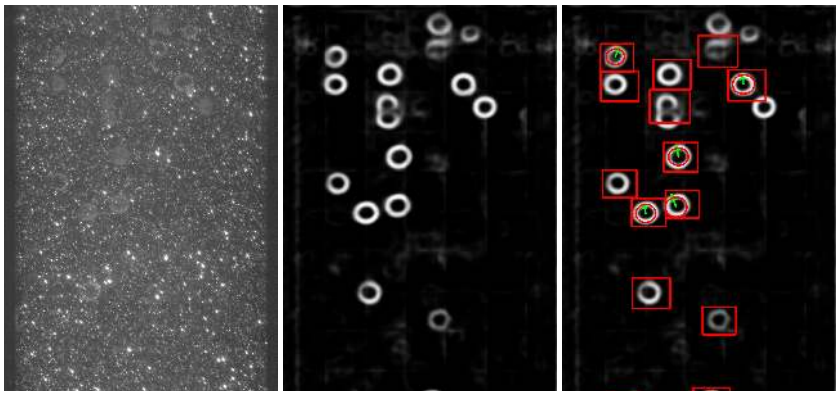

(b) Exp. 3

Figure 6: Examples of the identified bubbles through the model proposed in the present work. The leftmost image is the original PIV acquisition, the central image is the mask returned by the U-Net mode. The rightmost image shows the detected bubbles through the F-RCNN network and the instantaneous velocity calculated by the LOV technique.

In summary, the results of Fig. 6 show that the deep-learning based model is able to identify and extract information of the gas phase only by using the PIV acquisitions.

5.3 Experimental Validation

As a validation test, the average velocity of the dispersed bubbles $\overline{\langle \alpha_g \rangle}$ from Cerqueira *et al.* (2018), where the flow was analyzed through the PTV technique, are compared against the method detailed in the present work. Table 2 show the computed average rising bubble velocity and the difference $u_{b,diff}$ from the values obtained in Cerqueira *et al.* (2018). As observed, the values agree well in most of the studied experimental conditions, with only a single exception. That is the result of experimental condition 3 from Tab. 1, where the void fraction is the lowest. In this case that may be due to differences between the shadowgraphy method used in Cerqueira *et al.* (2018) and the PIV images used in the present work. Here, in the PIV images, the captured dispersed bubbles due to the planar illumination of the technique are located in the center plane of the test section. That is not the case in the shadowgraphy method, where the acquired bubbles are located throughout the entire pipe domain. Therefore, that may explain the large deviations found in this case.

Table 2: Comparison of the average dispersed bubble rising velocity calculate from the present deep-learning model and the results from Cerqueira *et al.* (2018).

Experiment No.	$j_l\ [m/s]$	$j_g\ [m/s]$	$\beta\ [-]$	$\overline{\langle \alpha_g \rangle}\ [-]$	$\overline{\langle u_b \rangle}\ [m/s]$	$u_{b,diff}\ [\%]$
1	$3.09 \cdot 10^{-2}$	$2.38 \cdot 10^{-3}$	0.084	0.013	0.189	3.82
2		$5.89 \cdot 10^{-3}$	0.160	0.029	0.190	-6.4
3	$21.64 \cdot 10^{-2}$	$2.38 \cdot 10^{-3}$	0.013	0.007	0.394	12.21
4		$9.66 \cdot 10^{-3}$	0.043	0.025	0.387	0.25

5.4 Average gas velocity profiles

Another advantage of the present method compared to the one detailed in Cerqueira *et al.* (2018), is the possibility to measure the bubble velocity close to the duct centre plane. As commented by Poletaev et. al. (Poletaev *et al.* (2016) and Poletaev *et al.* (2020)), when using a planar illumination, which is the case in the present work, one can assume that the dispersed bubbles are close to the laser light sheet. Therefore, Fig. 7 presents the average bubble rising velocity ($\langle w_g \rangle$) in the centre plane at a distance 70D away from the dispersed bubble inlet. Those results were ensembled averaged using the same methodology described in Cerqueira and Paladino (2021), where the bubble position and velocity are translated from a Lagrangian to an Eulerian reference frame.

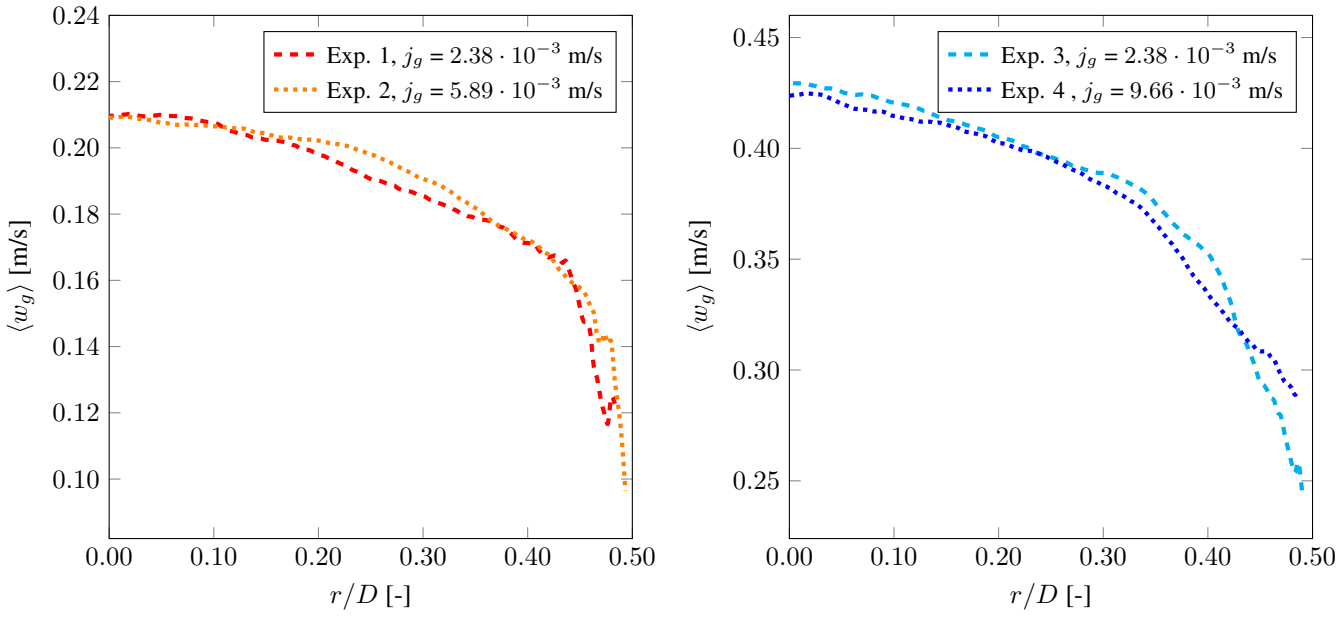

(a) $j_l = 3.09 \cdot 10^{-2}$ m/s (b) $j_l = 21.64 \cdot 10^{-2}$ m/s

Figure 7: Ensemble-averaged gas velocity profiles for the experiments given in Tab. 2 in the centre plane at a distance 70D away from the dispersed bubble inlet. The curves are divided into two separate plots, one for each j_l listed in Tab. 2.

As observed from Fig. 7, for the two j_l results, the shape of the average bubble velocity profile does not remain the same as j_g increases, following the average liquid velocity results described in Cerqueira *et al.* (2018). For the two cases presented in Fig. 7a), on average, as the gas void fraction increases, i.e., more bubbles are added, the terminal rising

velocity is increased. For experiments 3 and 4 of Tab. 2, Fig. 7b), the opposite trend is observed, indicating that the rising velocity may be reduced due to bubble interactions. A similar trend was observed in Garnier *et al.* (2002) and Simonnet *et al.* (2007). According to the authors, this modification is associated with the hindrance effect, caused by the combined effect of surrounding bubbles in a given bubble, which acts on the reduction of the terminal velocity in bubble swarms.

Another important observation from Fig. 7 is the modification of the average bubble velocity profiles close to the wall ($r/D > 0.40$). According to the results, the velocity profile in this region is affected by the global void fraction. However, by only analyzing the average bubble velocity profile, it is not possible to fully comprehend the modification of the bubble dynamics in this region. For a better comprehension, the results presented in Fig. 7 should be analyzed together with liquid phase velocity fields returned from the PIV technique.

6. CONCLUSIONS AND OUTLOOK

In this work, an algorithm based on the combination of different neural network architectures for the identification, labelling and shape fitting of bubbles in PIV images was presented. This algorithm is combined with a recently presented method for the determination o velocities of labelled objects in the images.

According to the experimental validation, the deep-learning method described here results in similar ensemble and spatial values as those obtained through the digital processing of shadowgraphy high-speed camera images. An advantage of the present methodology, due to the PIV's planar illumination, is the possibility to calculate ensemble average velocity profiles of the gas phase without a physical probe. The average bubble rising velocity profile shows that the rising velocity is affected by bubble interactions and this effect should further analyzed in future publications.

The method shows a promising application for the characterization of the bubbles' velocities, size and shape only from PIV acquisitions. Some improvements are still needed in the method. The segmentation process based on the U-Net model still outputs somewhat blurred bubble edges, and the F-RCNN still fails in detecting some of the bubbles present in the images.

Once optimized, these algorithms, in combination with the previous one presented in Cerqueira *et al.* (2021) will allow the full characterization of bubble flows, only from PIV acquisitions.

7. ACKNOWLEDGEMENTS

This work was partially supported by the ANP PRH-45 program.

8. REFERENCES

Abadi, M., Agarwal, A., Barham, P., Brevdo, E., Chen, Z., Citro, C., Corrado, G.S., Davis, A., Dean, J., Devin, M., Ghemawat, S., Goodfellow, I., Harp, A., Irving, G., Isard, M., Jia, Y., Jozefowicz, R., Kaiser, L., Kudlur, M., Levenberg, J., Mané, D., Monga, R., Moore, S., Murray, D., Olah, C., Schuster, M., Shlens, J., Steiner, B., Sutskever, I., Talwar, K., Tucker, P., Vanhoucke, V., Vasudevan, V., Viégas, F., Vinyals, O., Warden, P., Wattenberg, M., Wicke, M., Yu, Y. and Zheng, X., 2015. "TensorFlow: Large-scale machine learning on heterogeneous systems". URL `http://tensorflow.org/`. Software available from tensorflow.org.

Bank, D., Koenigstein, N. and Giryes, R., 2020. "Autoencoders". *arXiv preprint arXiv:2003.05991*.

Bradski, G., 2000. "The OpenCV Library". *Dr. Dobb's Journal of Software Tools*.

Bröder, D. and Sommerfeld, M., 2007. "Planar shadow image velocimetry for the analysis of the hydrodynamics in bubbly flows". *Measurement Science and Technology*, Vol. 18, No. 8, pp. 2513–2528. ISSN 0957-0233. doi:10.1088/0957-0233/18/8/028.

Bueno, R., Masotti, P., Justo, J., Andrade, D., Rocha, M., Torres, W. and de Mesquita, R., 2018. "Two-phase flow bubble detection method applied to natural circulation system using fuzzy image processing". *Nuclear Engineering and Design*, Vol. 335, pp. 255–264.

Cerqueira, R.F.L., Cerutti, M.A. and Paladino, E.E., 2021. "A deep-learning-based image processing technique for the measurement of two-phase bubbly flows using particle image velocimetry (PIV)". *"Proceedings of the 6th Multiphase Flow Journeys, 2021",*.

Cerqueira, R.F. and Paladino, E.E., 2021. "Development of a deep learning-based image processing technique for bubble pattern recognition and shape reconstruction in dense bubbly flows". *Chemical Engineering Science*, Vol. 230, p. 116163.

Cerqueira, R.F., Paladino, E.E., Brito, R.M., Maliska, C.R. and Meneghini, C., 2019. "Experimental apparatus and flow instrumentation for the investigation of a quasi-real slug flows in vertical ducts". *Experimental Thermal and Fluid Science*, Vol. 102, pp. 421–451.

Cerqueira, R., Paladino, E., Ynumaru, B. and Maliska, C., 2018. "Image processing techniques for the measurement of two-phase bubbly pipe flows using particle image and tracking velocimetry (PIV/PTV)". *Chemical Engineering Science*, Vol. 189, pp. 1–23. ISSN 00092509. doi:10.1016/j.ces.2018.05.029.

Chollet, F. *et al.*, 2015. "Keras". https://keras.io.

Chun-Yu, G., Yi-Wei, F., Yang, H., Peng, X. and Yun-Fei, K., 2021. "Deep-learning-based liquid extraction algorithm for particle image velocimetry in two-phase flow experiments of an object entering water". *Applied Ocean Research*, Vol. 108, p. 102526.

Garnier, C., Lance, M. and Marié, J., 2002. "Measurement of local flow characteristics in buoyancy-driven bubbly flow at high void fraction". *Experimental Thermal and Fluid Science*, Vol. 26, No. 6, pp. 811–815. ISSN 0894-1777. doi:https://doi.org/10.1016/S0894-1777(02)00198-X. URL https://www.sciencedirect.com/science/article/pii/S089417770200198X.

Haas, T., Schubert, C., Eickhoff, M. and Pfeifer, H., 2020. "BubCNN : Bubble detection using Faster RCNN and shape regression network". *Chemical Engineering Science*, Vol. 216, p. 115467. ISSN 0009-2509. doi:10.1016/j.ces.2019.115467.

Laupsien, D., Men, C.L., Cockx, A. and Line, A., 2021. "Labelled object velocimetry: Simultaneous measurements of bubble size and velocity". *Chemical Engineering Science*, Vol. 230, p. 116180. ISSN 0009-2509. doi:https://doi.org/10.1016/j.ces.2020.116180. URL https://www.sciencedirect.com/science/article/pii/S0009250920307120.

Poletaev, I.E., Pervunin, K.S. and Tokarev, M.P., 2016. "Artificial neural network for bubbles pattern recognition on the images". *Journal of Physics: Conference Series*, Vol. 754, p. 072002. ISSN 1742-6588. doi:10.1088/1742-6596/754/7/072002. URL http://stacks.iop.org/1742-6596/754/i=7/a=072002?key=crossref.988b278d1061eb6ebf9570fa8091b5a6.

Poletaev, I., Tokarev, M.P. and Pervunin, K.S., 2020. "Bubble Recognition Using Neural Networks: Application to the Analysis of a Two-Phase Bubbly Jet". *International Journal of Multiphase Flow*, p. 103194. ISSN 0301-9322. doi:10.1016/j.ijmultiphaseflow.2019.103194. URL https://doi.org/10.1016/j.ijmultiphaseflow.2019.103194.

Rasband, W.S. *et al.*, 1997. "Imagej".

Ronneberger, O., Fischer, P. and Brox, T., 2015. "U-net: Convolutional networks for biomedical image segmentation". In *International Conference on Medical image computing and computer-assisted intervention*. Springer, pp. 234–241.

Serra, P.L., Masotti, P.H., Rocha, M.S., de Andrade, D.A., Torres, W.M. and de Mesquita, R.N., 2020. "Two-phase flow void fraction estimation based on bubble image segmentation using randomized hough transform with neural network (rhtn)". *Progress in Nuclear Energy*, Vol. 118, p. 103133.

Simonnet, M., Gentric, C., Olmos, E. and Midoux, N., 2007. "Experimental determination of the drag coefficient in a swarm of bubbles". *Chemical Engineering Science*, Vol. 62, No. 3, pp. 858–866. ISSN 0009-2509. doi:https://doi.org/10.1016/j.ces.2006.10.012. URL https://www.sciencedirect.com/science/article/pii/S0009250906006622.

Torisaki, S. and Miwa, S., 2020. "Robust bubble feature extraction in gas-liquid two-phase flow using object detection technique". *Journal of Nuclear Science and Technology*, Vol. 57, No. 11, pp. 1231–1244.

Zhou, X., Doup, B. and Sun, X., 2013. "Measurements of liquid-phase turbulence in gas–liquid two-phase flows using particle image velocimetry". *Measurement Science and Technology*, Vol. 24, No. 12, p. 125303. ISSN 0957-0233. doi:10.1088/0957-0233/24/12/125303.

9. RESPONSIBILITY NOTICE

The authors are solely responsible for the printed material included in this paper.